Rapid Harmonic Analysis of Piezoelectric MEMS Resonators

Jonathan M. Puder[®], *Member, IEEE*, Jeffrey S. Pulskamp, Ryan Q. Rudy[®], Cristian Cassella, *Member, IEEE*, Matteo Rinaldi, *Senior Member, IEEE*, Guofeng Chen, *Student Member, IEEE*, Sunil A. Bhave, *Senior Member, IEEE*, and Ronald G. Polcawich, *Senior Member, IEEE*

Abstract—This paper reports on a novel simulation method combining the speed of analytical evaluation with the accuracy of finite-element analysis (FEA). This method is known as the rapid analytical-FEA technique (RAFT). The ability of the RAFT to accurately predict frequency response orders of magnitude faster than conventional simulation methods while providing deeper insights into device design not possible with other types of analysis is detailed. Simulation results from the RAFT across wide bandwidths are compared to measured results of resonators fabricated with various materials, frequencies, and topologies with good agreement. These include resonators targeting beam extension, disk flexure, and Lamé beam modes. An example scaling analysis is presented and other applications enabled are discussed as well. The supplemental material includes example code for implementation in ANSYS, although any commonly employed FEA package may be used.

Index Terms—Microelectromechanical systems (MEMS), modeling, piezoelectric, resonator, spurious mode.

I. Introduction

PIEZOELECTRIC radio frequency microelectromechanical systems (MEMS) resonators are a promising technology for meeting the increasing demands of a crowded electromagnetic spectrum while offering high integratability and low loss in an area efficient footprint. Contour-mode resonators are a potential technology for the next-generation filtering to replace current bulk acoustic wave (BAW) solutions.

Manuscript received October 8, 2017; accepted February 26, 2018. Date of publication April 2, 2018; date of current version June 1, 2018. This work was supported in part by an appointment to the Student Research Participation Program at the U.S. Army Research Laboratory administered by the Oak Ridge Institute for Science and Education through an interagency agreement between the U.S. Department of Energy and USARL. An earlier version of this paper was presented at the 2017 European Frequency and Time Forum and International Frequency Control Symposium and published in its proceedings [1]. (Corresponding author: Jonathan M. Puder.)

- J. M. Puder is with the Sibley School of Mechanical and Aerospace Engineering of Cornell University, and also with the U.S. Army Research Laboratory, Adelphi, MD 20783 USA (e-mail: jmp378@cornell.edu).
- J. S. Pulskamp, R. Q. Rudy, and R. G. Polcawich are with the U.S. Army Research Laboratory, Adelphi, MD 20783 USA (e-mail: Jeffrey.s. pulskamp.civ@mail.mil; ryan.q.rudy.civ@mail.mil; Ronald.g.polcawich.civ@mail.mil).
- C. Cassella, M. Rinaldi, and G. Chen are with the Electrical and Computer Engineering Department of Northeastern University, Boston, MA 02052 USA (e-mail: cristian.cassella@broadcom.com; rinaldi@ecc.neu.edu; chen.guof@huskv.neu.edu).
- S. A. Bhave is with the Electrical and Computer Engineering Department of Purdue University, West Lafayette, IN 47907 USA (e-mail: bhave@purdue.edu).

This paper has supplementary downloadable material available at http://ieeexplore.ieee.org, provided by the authors.

Digital Object Identifier 10.1109/TUFFC.2018.2822119

The lithographically defined center frequencies of contourmode resonators facilitate monolithic integration of multiple frequencies on a single chip, ideal for filter bank applications.

Despite these advantages, the contour-mode resonator technology has not seen widespread use in commercial or military applications. One of the main obstacles toward this end is the spurious mode problem [2]–[5]. This was a major problem the BAW community needed to solve before successful commercialization [6]. Continuum distributed mechanical systems theoretically have an infinite number of natural modes. Frequently, electrodes designed to optimally excite an intended mode will also excite several other (spurious) modes. This can affect the passband roll-off and group delay of filters created from these resonators, and potentially exposes the radio system to damaging high-power signals at frequencies far from the intended frequency.

Part of the reason spurious modes remain a challenge is the lack of a rapid and wide-band simulation technique. Piezoelectric resonators typically have complex geometries with nonanalytical mode shapes and complex electric fields that must be modeled using finite-element analysis (FEA) for accuracy. Conventionally, a multiphysics harmonic analysis is run to model resonators [7]. For these simulations, the full equations of state must be solved at every single frequency point for which information is desired. These simulations can take hours to days to complete, and sometimes longer [7]. Trades must be made between frequency spacing and bandwidth for the simulation to complete in a reasonable amount of time. This technique is susceptible to missing resonances if frequency point spacing is too wide. Due to the time limitations, designers often run 2-D simulations, which complete much faster [3], [5], but will miss any out-of-plane information, such as modes propagating out of plane, or strain variation along that direction.

To address these challenges, the wide-band rapid analytical-FEA technique (RAFT) has been developed using software commonly found in research laboratories [1]. The RAFT combines the speed of analytical analysis with the accuracy of FEA for full 3-D solutions that complete orders of magnitude faster than conventional harmonic analysis while accurately modeling all modes. In this case, the software used is ANSYS and MATLAB; however, it may be implemented in any other FEA/analytical package desired. This enhanced speed is enabled by generalized expressions for the motional parameters of the modified Butterworth van-Dyke equivalent

circuit [8]: motional resistance (R_m) , inductance (L_m) , and capacitance (C_m) .

To simulate the frequency response, first information from an FEA modal analysis and an electrostatic analysis are used in the generalized equations for the motional parameters, effectively reducing the number of frequency points that must be simulated in FEA to only those where mechanical modes exist. Next, the mechanical quality factor Q_m must be set for each mode. Other modified Butterworth van-Dyke (mBVD) parameters such as capacitances and resistances must be set. After this is completed, the full frequency response of the resonators may be quickly simulated in an analytical software package which performs the modal superposition.

This method is shown to improve simulations speeds by several orders of magnitude. In addition to the improved modeling of spurious response, the RAFT enables new uses of FEA for design and analysis. Wide-band simulations to assess the resonator performance far from resonance are now possible [1]. Accurate para metric device exploration to investigate mode scaling and behavior to higher frequencies can be undertaken [9]. The reduced simulation duration frees time for researchers to conduct studies of other critical device variables, such as the simulations of fabrication nonidealities, including electrode misalignment or sidewall angles. These effects are often not simulated due to time constrains. Thermal effects on frequency may be included to generate frequency—temperature curves for each mode's unique response to temperature variations. Also, novel modes may be investigated.

The modeling methodology is applicable to other resonant systems as well, such as gyroscopes, ultrasonic motors, strain sensors, and oscillators, but detailed discussion is beyond the scope of this paper.

The remainder of this paper is arranged as follows. Section II discusses in detail the components of RAFT, its implementation, and advantages. It will include a presentation of the most general mBVD motional parameter equations with complex electric fields, as well as a general expression for the electromechanical coupling $k_{\rm eff}^2$. Section III contains experiment details. Section IV presents validation and applications of the RAFT, including wide-band frequency simulations and parametric device exploration. Section IV draws the conclusion. The Appendix provides an alternate derivation of the motional parameters of the mBVD.

II. MODELING

This section discusses various components of the RAFT individually, and gives details on how they are combined into a unified modeling technique.

A. Modified Butterworth Van-Dyke Model

The mBVD model is a well-known equivalent circuit model for piezoelectric resonators, and is instrumental in developing this simulation technique [8]. It is discussed here to clarify its use in the simulation technique. The mBVD for one and two-port resonators is shown in Fig. 1(a) and (b). Capacitors C_0 (one-port) and C_1 and C_2 (two-port) are formed by the electrodes of the piezoelectric resonator. The $R_{\rm teth}$ are the

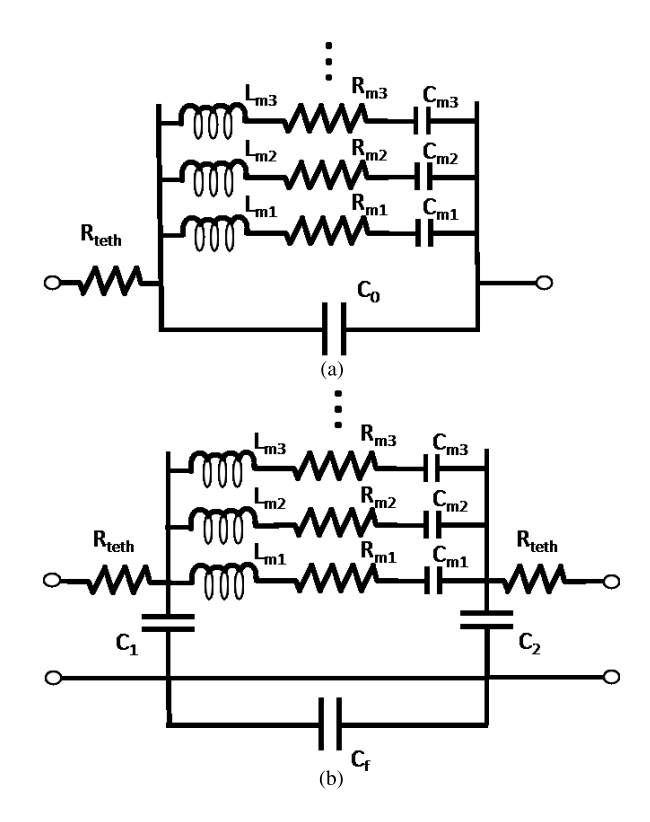


Fig. 1. mBVD model for (a) one-port resonators and (b) two-port resonators.

resistance of the electrical routing to the device. C_f is the feed-through capacitance, which is the mutual capacitance between the electrodes of the two ports. The motional arm, consisting of the motional resistance, inductance, and capacitance, is the electrical equivalent of the lumped mass-spring-damper model with coupling incorporated. Modal analysis is used to superimpose the response of each mode to obtain a full frequency response [10]. This is accomplished in the mBVD by placing motional arms in parallel. In this way, each mode experiences the same applied voltage, but produces a different motional current depending on resonance conditions and coupling.

B. Generalized Motional Parameters

The derivation of the motional parameters in this paper is different compared to the derivation in [11]. A derivation similar to that of [11] is included in the Appendix. In this derivation, a uniform electric field between two parallel plates is no longer assumed, and a generalized "turns ratio" is explicitly given [12]. This seemingly minor distinction is quite significant, as higher frequency applications demand the use of interdigitated transducers (IDTs) [13]-[15]. These transducers produce complex electric fields that can be difficult to model analytically. The shape of this electric field determines the interaction with the strain field, and therefore is directly related to coupling. Similar to the derivation in [11], the assumptions from modal analysis that the modes are not strongly coupled and therefore solutions are linearly independent, and that a distributed system may be represented as a lumped system, are fundamental to this analysis. In addition, another assumption inherent in this analysis is that the undamped mode shapes

are an excellent approximation for the damped modes shapes. This is valid for modes with low damping.

The quasi-static total internal energy of a system may be written as a summation of the energy stored purely elastically (U_e) , purely electrically (U_d) , and the mutual energy stored as a consequence of the piezoelectric effect (U_m) [16]. The mutual energy represents the additional energy stored elastically when an electric field is applied to a piezoelectric creating mechanical displacement, as well as the consequent additional energy stored capacitively due to the increased polarization from the strained piezoelectric (hence the factor of 2)

$$U = U_e + 2U_m + U_d. (1)$$

Modal analysis allows the treatment of a single mode independently of all other modes for mechanical modes with low damping and negligible coupling. The full frequency response is then a superposition of these individual contributions. Therefore, the energy of a single arbitrary mode is considered and expressions kept are generalized to apply to any mode. Considering the energy of a single, arbitrary mode, the energies of that mode are defined as

$$U_e = \frac{1}{2} \delta^2 \int_V \mathbf{S}_n \times \mathbf{c}^E \times \mathbf{S}_n dV \tag{2}$$

$$U_m = \frac{1}{2} \Phi \delta \int_{V} e^t \times \nabla \phi \times \mathbf{S}_n dV$$
 (3)

$$U_d = \frac{1}{2} \Phi^2 \int_V (\nabla \phi) \times \epsilon^T \times (\nabla \phi) dV. \tag{4}$$

Here, δ is the modal displacement, which is defined to be the point of maximum displacement on the resonator for the particular mode. S_n is the unity normalized strain written in 6-D vector notation (therefore, δS_n is the real strain), c^E is the stiffness matrix at constant electric field, Φ is the magnitude of the applied voltage, ϕ is the unity normalized potential field (therefore, $\Phi \nabla \phi$ is the real electric field), ϵ^T is the permittivity at constant stress, and V is the volume of the resonator. (Note that U_m is only nonzero in the piezoelectric.)

The derivation is performed in the quasi-static case, in which a voltage is applied to the electrodes of a resonator. The frequency-dependent equations may be generated by multiplying the relevant expressions by

$$u_t = \frac{e^{j\omega t}}{\left(1 - \frac{\omega^2}{\omega_n^2}\right) + \frac{j\omega}{Q_m \omega_n}} \tag{5}$$

where ω is the drive frequency, ω_n is the natural frequency, and Q_m is the mechanical quality factor of the particular mode.

In the quasi-static case, the mutual energy is understood to account for both the mechanical potential energy stored from the displacement/strain of the beam and the additional charge that is stored on the electrode due to the increased polarization caused by the mechanical displacement. U_e accounts for energy from purely elastic effects. U_d represents the energy that is stored purely from dielectric effects. Therefore, only the mutual energy is considered when analyzing coupling between domains. This energy is then modeled by a lumped modal spring with an applied modal force (to represent the

electric field causing a displacement) and a lumped modal capacitor with an applied voltage (to represent the additional charge stored from the increase in polarization caused by displacement). The energy from these lumped parameters is equated to the total mutual energy

$$\frac{1}{2}F_m\delta + \frac{1}{2}Q\Phi = \Phi\delta \int_V e^t \times \nabla\phi \times S_n dV \tag{6}$$

where F_m is the modal force and Q is the charge on the modal capacitor.

Dividing both sides of (6) by δ and Φ returns

$$\eta = \frac{1}{2} \frac{F_m}{\Phi} + \frac{1}{2} \frac{Q}{\delta} = \int_V e^t \times \nabla \phi \times S_n dV \tag{7}$$

where η is the "turns ratio" for the transduction of voltage to modal force and displacement to charge on the same port, and is defined to be the ratio of modal force to voltage or the ratio of charge to modal displacement (or current to modal velocity) [12].

From [12], the motional parameters are

$$R_m = \frac{b_m}{\eta_1 \eta_2} \tag{8}$$

$$C_m = \frac{\eta_1 \eta_2}{k_m} \tag{9}$$

$$L_m = \frac{m_m}{\eta_1 \eta_2} \tag{10}$$

where k_m , m_m , and b_m are the modal stiffness, mass, and damping. The subscripts on η are used to distinguish the case where the input and output electrodes (ports) are different. The modal mechanical parameters are given by

$$k_m = \int_{V} \mathbf{S}_n \times \mathbf{c} \times \mathbf{S}_n dV \tag{11}$$

$$m_m = \int_V \rho(x, y, z) u_n^2 dV \tag{12}$$

$$b_m = \frac{k_m}{Q_m \omega_n} = \frac{m_m \omega_n}{Q_m} \tag{13}$$

where ρ is the density and u_n is the unity normalized mode shape. Using (7) and (13) in (8) returns the motional resistance, given by

$$R_{m} = \frac{k_{m}}{Q_{m}\omega_{n} \int_{V} \mathbf{e}^{t} \times \nabla \phi_{\text{in}} \times \mathbf{S}_{n} dV \int_{V} \mathbf{e}^{t} \times \nabla \phi_{\text{out}} \times \mathbf{S}_{n} dV}.$$
(14)

This is the most general form of the motional resistance, and is valid for any topology, material, or mode, provided all assumptions have been met. For a two-port resonator, the two integrals in (14) may have different signs depending on where the electrodes are placed on the resonator. Note that with parallel plate topology (i.e., $\nabla \phi = [(1/t_{\text{piezo}})00]'$, where t_{piezo} the thickness of the piezoelectric), (14) reduces to the expression given in [11].

 L_m and C_m are derived by inserting (7) into (9) and (10)

$$L_m = \frac{m_m}{\int_V e^t \times \nabla \phi_{\text{in}} \times S_n dV \int_V e^t \times \nabla \phi_{\text{out}} \times S_n dV}$$
 (15)

$$C_m = \frac{\int_V e^t \times \nabla \phi_{\text{in}} \times S_n dV \int_V e^t \times \nabla \phi_{\text{out}} \times S_n dV}{k_m}.$$
 (16)

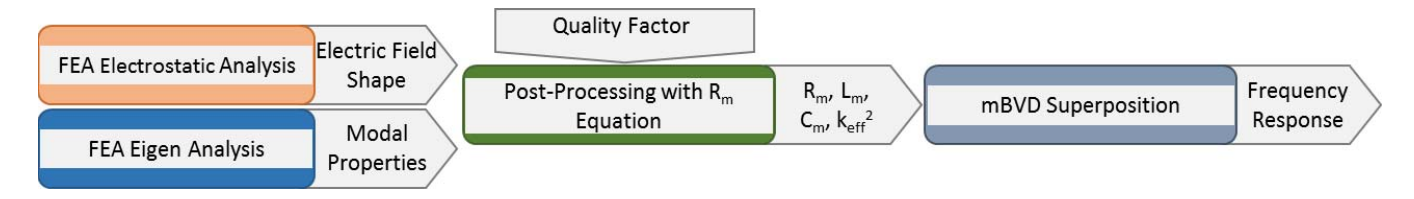


Fig. 2. Graphical overview of the RAFT. First, FEA Eigen and electrostatic analyses are run. This information is entered in the generalized motional parameters, and the quality factor is set. Finally, the modes are superimposed using the mBVD in an analytical software package to simulate the frequency response.

When (16) is placed in the equation for k_{eff}^2 , it gives a convenient expression to predict coupling [17]

$$k_{\text{eff}}^{2} = \frac{1}{\frac{C_{0}}{C_{m}} + 1}$$

$$= \frac{1}{\frac{k_{m}C_{0}}{\left|\int_{V} e^{t} \times \nabla \phi_{\text{in}} \times S_{n} dV \int_{V} e^{t} \times \nabla \phi_{\text{out}} \times S_{n} dV\right|} + 1}$$
(17)

where C_0 is the shunt capacitance for a one-port resonator, or the equivalent capacitance of C_1 and C_2 (Fig. 1) when placed in series to create an equivalent one-port resonator (Fig. 1) as in [18]. Note that, this expression requires no knowledge of the frequency response. In harmonic analyses, the $k_{\rm eff}^2$ is often obtained by fitting the mBVD model to the resonator, simulating that fit resonators frequency response, and then using

$$k_{\text{eff}}^2 = \frac{f_a^2 - f_r^2}{f_a^2} \tag{18}$$

where f_a is the antiresonant frequency and f_r is the resonant frequency [17].

The first thing to note for these expressions is that they are symmetric, i.e., these expressions represent a reciprocal system. Second, the spatial interaction of the electric field and the strain is important. Ideally, they have the same shape to maximize their dot product. Any strain that is not directly transduced to/from the electric field serves only to increase the motional stiffness, thereby increasing R_m and reducing coupling, a point elaborated upon in [11] and [18]. Also, the expression for $k_{\rm eff}^2$ does not require any knowledge about the frequency response; if the electric field and strain are known, it may be calculated directly from that information. Finally, L_m and C_m (and hence the coupling) are both unaffected by the quality factor of the device, while R_m is inversely proportional to quality factor.

C. Predicting Displacement and Charge

The real displacement and charge produced by a piezoelectric on an elastic layer are useful in many applications such as strain sensors, ultrasonic motors, actuators, and gyroscopes. These expressions are derived in the Appendix as substeps to an alternate derivation of the motional parameters, and are specifically called out here. To the best of the author's knowledge, this is the first time that such closed form expression has been presented. They have not been experimentally verified. However, a similar methodology was used for modeling the dynamics of an actuator used for switching [19].

This approach used a specific expression for the modal force to predict the displacement of each mode, and superimposed these displacements to predict time-domain switch dynamics with good agreement.

For a particular mode, the charge appearing on the output port due to an applied strain and displacement caused by an applied electric field are predicted by

$$\delta = \frac{F_m}{k_m} = \frac{\int_V \mathbf{e}^t \times \Phi \nabla \phi \times \mathbf{S}_n dV}{k_m} \tag{19}$$

$$Q_{\text{out}} = \int_{V} \boldsymbol{e} \times \delta \boldsymbol{S}_{n} \times \nabla \phi_{\text{out}} dV. \tag{20}$$

Here, δS_n is the real spatial component of strain, and $\Phi \nabla \phi$ is the real electric field across the input port. The time varying charge and displacement magnitude may be expressed by multiplying (19) and (20) by (5).

D. Rapid Analytical-FEA Technique

The major components of the RAFT have been discussed, and this section ties them together and discusses the difference between the conventional harmonic analysis. Fig. 2 gives a graphical overview of the RAFT.

The RAFT assumes small piezoelectricity [20]–[22]. With small piezoelectricity, the electric field contribution from mechanical strains is considered negligible, and the purely elastic solution to the wave equation is considered a good approximation to the solution from the piezoelectric wave equation.

The purely mechanical modal properties are obtained via an Eigen analysis. This delivers the modal strain and natural frequency, as well as the total mechanical energy and maximum normalized displacement, which are used to obtain the modal stiffness. An electrostatic simulation returns the shape of the applied electric field. This simulation can also return any shunt and/or parasitic capacitances for use in the mBVD model. At this point, the only unknown information is Q_m , which must be measured, assumed, or modeled. The modeling of quality factor is outside of the scope of this paper. Methods exist in the FEA packages for modeling Q_m , such as structural damping models, viscous damping models (compatible with modal analysis), and perfectly matched layers. Next, analytical evaluation software is utilized to generate network parameters by either directly generating admittance/impedance or first evaluating the circuit into ABCD parameters, and then converting the parameter of choice.

The RAFT minimizes reliance on computationally intensive simulation by using the generalized motional parameters and mBVD model to reduce the required number of simulated frequency points and separate the simulation of the mechanical and electrical domains. Apart from the above, this approach has multiple additional major benefits over multiphysics harmonic analysis for simulation speed and insight.

Relating to simulation speed, there are several other advantages. First, the electrical component of the problem is only solved once to obtain the shape of the electric field, as opposed to harmonic analysis where it is effectively solved at every frequency step. Second, the completion time of the RAFT is proportional to the number of modes in the simulation band. With harmonic analysis, every single-frequency point for which information is desired must be simulated, which is generally denser than the spacing of modes. Finally, the RAFT returns the electromechanical coupling without requiring the frequency response to be generated (17).

Relating to insight, first the RAFT will not miss modes by the nature of Eigen analysis, provided a dense enough mesh is used. Harmonic analysis can potentially miss or distort information if frequency points are not appropriately chosen. Second, designers may attribute contributions to the frequency response to individual modes. The motional resistance and coupling of every single mode is returned before frequency response generation. This allows the designer to pick out exactly which modes are interfering with the desired response. In harmonic analysis, the results obtained are a superposition of all modes at each frequency, and can be difficult to decouple. Third, designers may distinguish between contributions to coupling from individual piezoelectric constants. For example, the RAFT allows designers to quantify the amount of coupling from e_{33} versus e_{31} to the overall coupling, or any other constant of interest. Finally, the RAFT allows the designer to set the Q and pie zoelectric constants after all FEA simulations have been run. This is particularly useful for ferroelectrics for which the piezoelectric constants, dielectric constants, and even the Q are dependent on an applied dc bias field. In addition, the designer may assign Q based on whatever criteria or model they choose.

III. EXPERIMENT

To demonstrate the flexibility of this modeling method, devices based on PZT or AlN are analyzed at frequencies as low as 1 MHz and as high as 800 MHz in various shapes and with various electrode designs. This demonstrates the model is accurate across materials, frequencies, and topologies.

PZT-on-silicon devices have shown high performance at frequencies below 200 MHz [23], [24], a frequency range utilized for many military applications. This performance is in part due to the high piezoelectric constants of PZT [25], [26]. Thin-film PZT tends to be a low *Q* material, and therefore silicon is incorporated into the resonators to boost the *Q* at the cost of electromechanical coupling.

Aluminum nitride (AlN) is often the top choice for high-frequency applications due to its high acoustic velocity, low loss, and well developed and repeatable processing [27]. The AlN cross-sectional Lamé-Mode resonators (CLMRs) modeled in this paper have shown high coupling and quality factors at higher frequencies [28], [29]. The Lamé mode is a primarily

a 2-D mode, since in the ideal case only two nonzero directions of strain exist.

For the fabrication of the PZT-on-silicon resonators analyzed in this paper, the author refers the reader to [30]. For the fabrication of the AlN resonators analyzed in this paper, the author refers the reader to [18].

A. Computer and Software Specifications

All simulations were run on machine running Windows 7 Enterprise with 32 GB of memory. The processor is an Intel Xeon E5-2620 CPU.

FEA simulations were performed in ANSYS 15.0 using the mechanical APDL interface. APDL was used to allow easy parameterization of designs for scaling studies, as well as simplify the automated saving of data. MATLAB R2015a was used for analytical evaluations of the mBVD and parsing of data.

Example code is provided as a supplemental file for the APDL/MATLAB implementation of the simulation of the CLMR bar resonator. It should be noted that it is not necessary to use the software, in which this technique was implemented. It is possible to implement this in any FEA package capable of Eigen analysis and electric field simulation, and any analytical software.

B. Device and Measurement Details

The frequency response of three resonator geometries is analyzed. The first is a PZT-on-Si bar resonator intended to excite the sixth harmonic of length extension. The second is a PZT-on-Si disk resonator, intended to excite the (1, 1) mode of disk flexure. Devices based upon this mode have shown -1 dB of loss in a recent publication [24]. Both resonators have a two-port topology. The third resonator is an AlN bar CLMR with top and bottom IDT electrodes, which has demonstrated low impedance, high coupling and high quality factor [30].

The PZT-on-silicon resonators were tested using a ZVB-8 network analyzer terminated to 50 Ω and calibrated using a through, open, short, and load standard (GGB CS-5). The two-port scattering (S) parameters were measured. Nonmotional mBVD properties were obtained via extraction. For the capacitance and tether resistance, the Z_{11} parameter was examined away from resonance. The real part of Z_{11} was affected by the tether resistance as well as the real component of the impedance of the shunt capacitor. These effects are distinguishable due to the frequency dependence of the impedance change due to a lossy dielectric. The tether resistance was assumed to remain constant across frequency. The feed-through capacitance [Fig. 1(b)] was small compared to C_1 and C_2 , and therefore neglected.

The material properties of the PZT-on-silicon resonators were independently measured [32]. The e_{31} constants were fit to the data, but fell within values extracted from on-after cantilever test structures [26]. Lateral device dimensions were taken from design, and modified slightly for frequency agreement, resulting in a 0.5- μ m decrease in disk radius and beamwidth. Layer thicknesses were taken from nominal deposition values. The material stack consists of 1- μ m buried

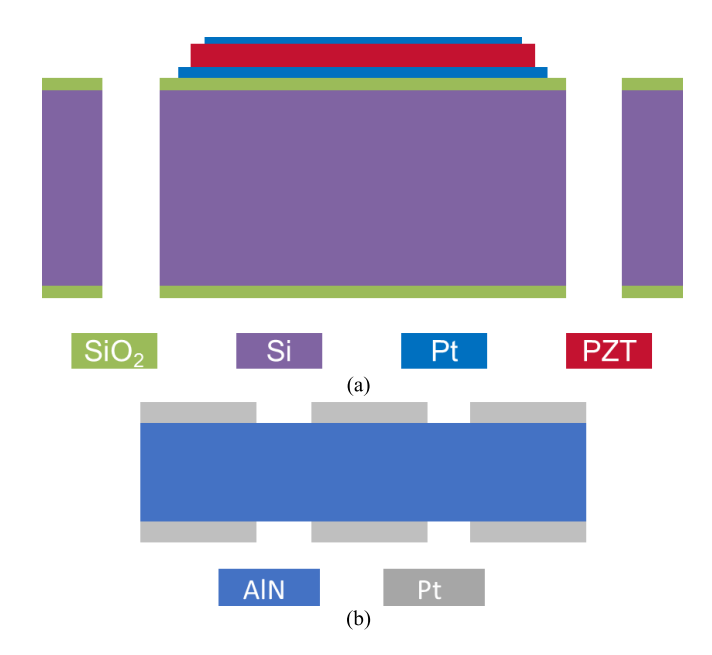


Fig. 3. Cross-sectional view of the (a) material stacks for the PZT-on-silicon resonators and (b) aluminum nitride CLMRs.

silicon dioxide, 10 μ m of silicon, 300 nm of silicon dioxide, 125 nm of platinum, 0.5 μ m of PZT, and 50 nm of platinum [Fig. 3(a)].

PZT-on-Si resonators generally show the best performance below 200 MHz, where the electrodes generally have a parallel plate topology. The equation for motional resistance presented in [11] is applicable

$$R_m = \frac{k_m}{Q_m \omega_n |\int_{A_{\text{in}}} \mathbf{e} \times \overline{\mathbf{S}}_n dA \int_{A_{\text{out}}} \mathbf{e} \times \overline{\mathbf{S}}_n dA|}.$$
 (21)

Since a constant electric field is assumed, no simulation of the electrical domain was performed.

The CLMRs were measured using an Agilent 5071C vector network analyzer and Cascade Microtech ground–signal–ground probes in air at room temperature. Calibration was performed on reference substrate using a short, open, and load standard. In addition, pad capacitances were de-embedded to obtain performance attributable directly to the device [33].

Material properties were obtained from the default COMSOL material library. AlN thickness was obtained using a Nanospec Spectrophotometer, and the platinum thickness was obtained using a Dek-tak 3030/3St stylus profilometer. These resulted in thicknesses of 0.3, 4, and 0.3 μ m for the Pt–AlN–Pt stack [Fig. 3(b)].

IV. RESULTS

A. Beam PZT-on-Silicon Resonator

The beam extension device was measured from 1–80 MHz, with the designed mode at 20.7 MHz. Agreement between the measurement and results from RAFT is presented in Fig. 4. The Q_m was taken directly from measurement where possible. Other modes had fit Q_m due to extraction difficulty from loss or adjacency to other modes. The RAFT accurately predicted device behavior across a wide range of frequencies. The modal analysis indicated that there are a total

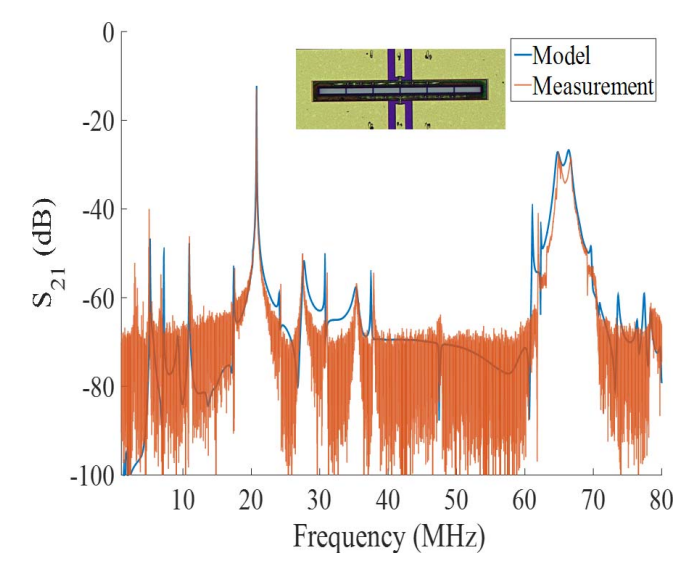


Fig. 4. RAFT results for a beam extension resonator intended to operate in its sixth harmonic.

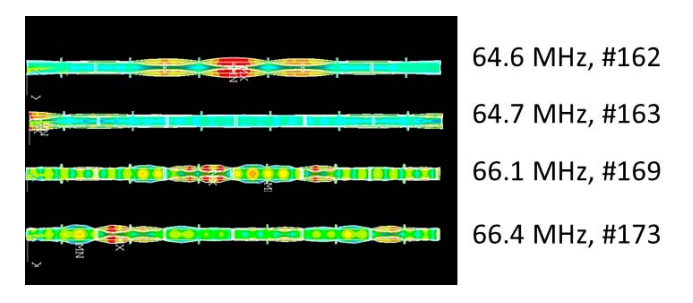


Fig. 5. Four highest coupling modes in the pseudopassband of Fig. 3. RAFT allows designers to pick out individual modes, which are contributing the most to spurious responses. The number next to each mode is the number out of the 247 spurious modes when modes are organized from lowest to highest frequency.

of 247 modes in the simulated frequency span. This simulation took 9.9 min to complete with $345\,000^\circ$ degrees of freedom. Across modes with measured Q_m , the average error was approximately 1.5 dB. For the intended mode at 20.4 MHz, the error was 1.4 dB.

In Fig. 4, there is a pseudopassband from \sim 60–70 MHz. The RAFT shows there are 15–20 harmonics of width flexure creating this undesirable behavior. These harmonics are at slightly different frequencies due to the tether modifying local stiffnesses. With RAFT, it is possible to identify the modes with largest coupling. These modes may be seen from Fig. 5.

B. Disk Flexure PZT-on-Silicon Resonator

The disk flexure-based devices were measured from 1 to 100 MHz, with the intended mode at 20.65 MHz. Eigen analysis indicates that there are 103 modes in this frequency range. The RAFT generated and measured frequency response may be seen from Fig. 6. Again, close agreement with the measurement is observed. As with the beam example, Q_m was taken from measurement where possible. Across modes with fit Q_m , the average error at resonance was 1.5 dB. The error for the intended mode at 22.6 MHz was 0.35 dB. For the disk,

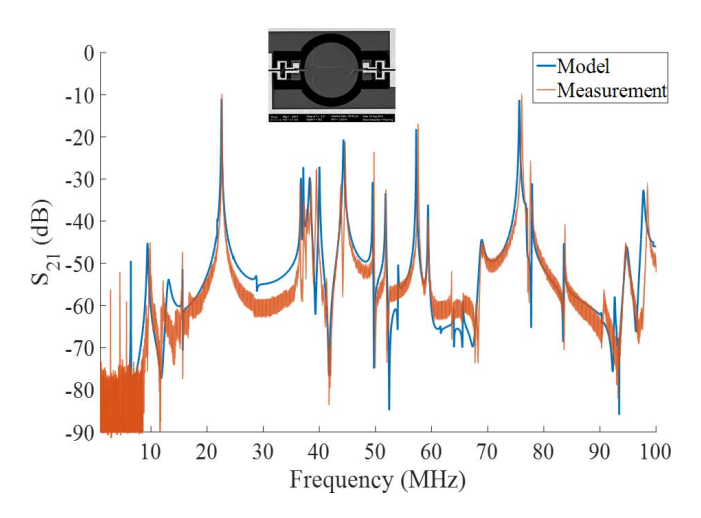


Fig. 6. RAFT results for a disk resonator designed to optimally excite the (1, 1) mode of disk flexure.

TABLE I SIMULATION AND DEVICE CHARACTERISTICS

Device Name	Pitch (µm)	QuL	Measured Min Impedance (Ω)	Min	Meas. Cm	RAFT C _m (fF)	RAFT k _{eff} ²
A1	5.0	2820	39.9	45.7	1.76	1.87	3.69
A2	5.2	2493	43.8	50.0	1.77	2.00	3.79
A3	5.4	2977	39.0	38.9	1.97	1.90	3.94

the time from simulation start to generation of S-parameters was 11.7 min with \sim 460 000 degrees of freedom.

C. Beam AlN CLMR

Three separate beam CLMR designs which had previously been presented in [34] were analyzed. The primary difference between is the pitch of the IDT electrodes. The device characteristic may be seen from Table I. Since the elastic moduli and densities were not measured, the simulated center frequencies were not well matched to the measured frequencies. Therefore, each simulation band was shifted by 8.29%, 7.16%, and 6.13% for devices A1, A2, and A3, respectively. For the simulation results, all modes were set to have identical Q_m to that of the main resonance. The results from these simulations may be seen from Fig. 7.

The simulations took an average of 26 min to complete. As mentioned previously, the RAFT's completion time is proportional to the number of modes in the simulation bandwidth. At higher frequencies, the number of spurious modes increases drastically. This results in a decrease speed for the RAFT in terms of bandwidth simulated per minute. To allow for rapid modeling, a mesh such as that show in Fig. 8 was utilized. The mesh is coarse in the length, but fine along the width and the thickness. A similar approach to meshing was taken in [6].

After the center frequencies are aligned and the Q_m are set to the measured value, excellent agreement is seen between the measurement and simulation. One of the reported benefits of CLMRs is ability to coherently transduce using both e_{31} and e_{33} [30]. RAFT confirms this numerically. The RAFT

TABLE II Simulation Times for 99-MHz Bandwidth of Disk Flexure Resonator

Points	Frequency Resolution	COMSOL Simulation Time	RAFT Simulation Time	tcomsoi/traft
9900	10 kHz	~10d 5h 30m	11.7m	1259
49500	2 kHz	~54d 10 h	11.7m	6697
99000	1 kHz	~112d 7h	311.7m	13820

predicts e_{31} contributes 17.3%, 19%, and 21.2% of the total coupling for devices A1, A2, and A3, respectively. For coupling comparison, the C_m from RAFT and the results from fitting an mBVD to measured data are presented in Table I. The percent error in C_m for each resonator was 5.9, 11.5, and 3.6. The coupling predicted by RAFT was calculated using (17) and (18). Both methods agreed within half a percent. The calculated $k_{\rm eff}^2$ are 3.69%, 3.79%, and 3.91% for A1, A2, and A3, respectively. These results, along with the minimum simulated and measured impedances are reported in Table I.

Due to frequency disagreement between measurement and simulation, there was difficulty attributing modes in simulation to modes in measurement. This is mostly attributed to uncertainty in the material properties, as previously it was stated that the default material library from COMSOL was used to set values. Therefore, all modes were set to have the same Q_m as the main resonance. The frequency disagreement also creates difficulty drawing a conclusion about the accuracy of the spurious modes modeled.

D. Comparison to Harmonic Analysis

To illustrate the speed of this method, a COMSOL harmonic analysis simulation was compared to the RAFT for the disk flexure resonator from Section II. Simulating the full frequency spectrum with harmonic analysis is not feasible, and so several shorter runs were performed and timed. A time per frequency point was calculated and linearly extrapolated. Table II compares the time to completions for the disk resonators over the 99-MHz bandwidth for models with 460 000 degrees of freedom ($t_{\rm COMSOL}$ and $t_{\rm RAFT}$). For context, a 1-kHz frequency resolution will place approximately 35 points in the bandwidth.

E. Discussion

The RAFT has demonstrated significant reduction in simulation speed when compared to conventional harmonics analysis. The numerous other advantage have been exhibited as well, namely, direct calculation predicted coupling without the requirement of simulating frequency, ability to attribute coupling to particular piezoelectric constants, and the inherent quality of the RAFT of not missing modes.

One caveat must be observed when utilizing RAFT: if a low loss mode is just outside the bandwidth simulated, the effect of that mode will not be included in the simulated frequency response at all. This is on disadvantage that harmonic analysis does not have, as the full equations of state are solved at each frequency point. Therefore, it is prudent to simulated frequencies outside the bandwidth of interest as well.

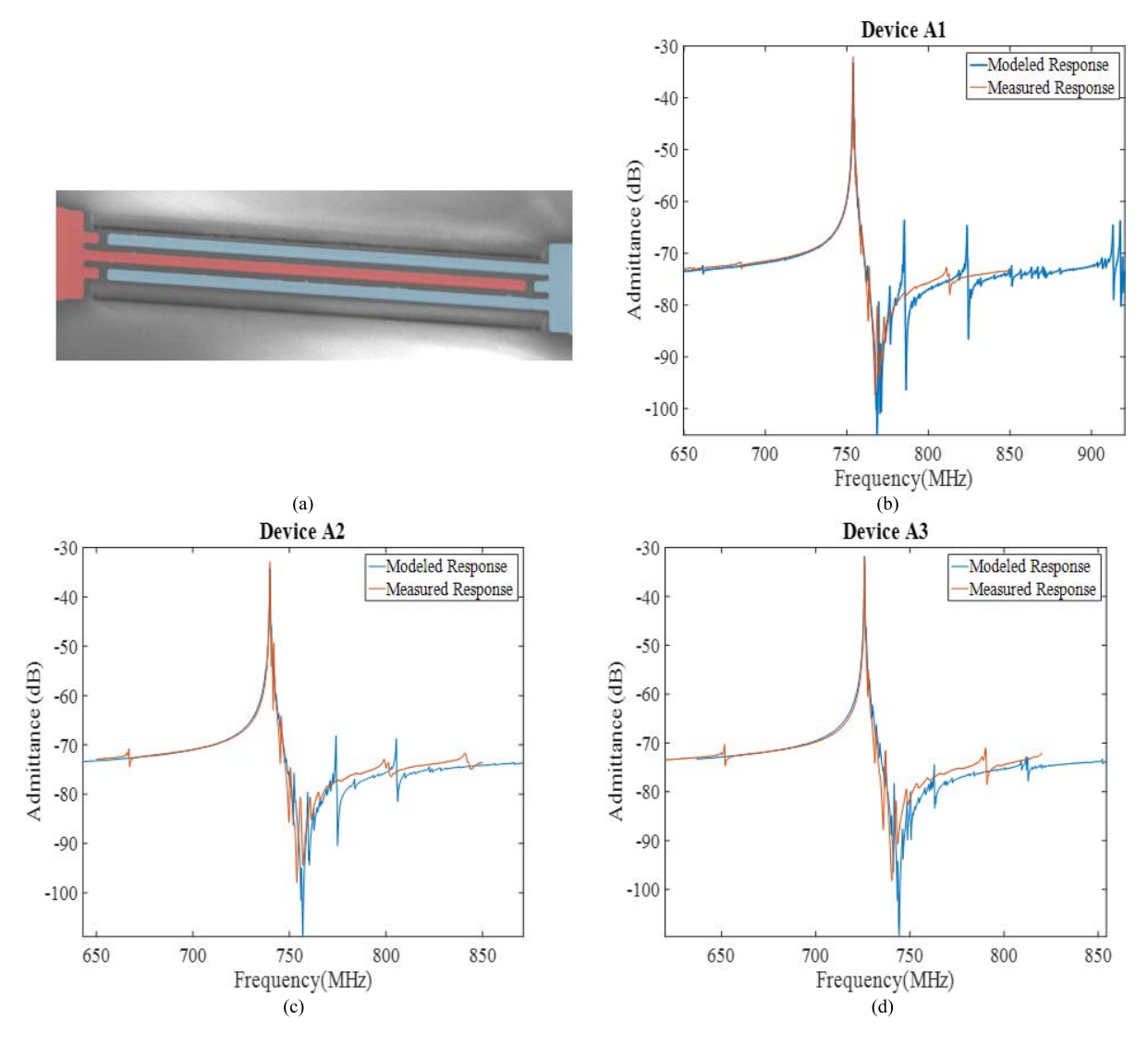


Fig. 7. (a) Scanning electron micrograph of a CLMR. The red and blue denote the ground and signal electrodes. The simulation results for (b) device A1, (c) device A2, and (d) device A3 AlN CLMR resonators. The results from the RAFT were scaled up in frequency for comparison due to uncertainties in the material properties.

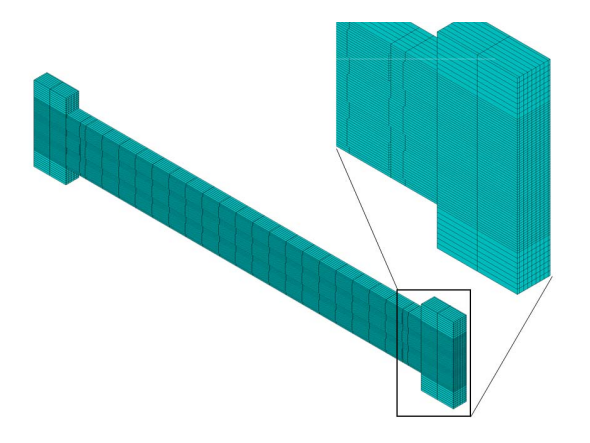


Fig. 8. Image of the mesh used for the CLMRs.

V. CONCLUSION

The RAFT has been demonstrated, showing a significant reduction in simulation times. Example code has been provided as supplemental material for implementation in ANSYS using the ANSYS Parametric Design Language and MATLAB. The code is relatively short and straightforward. Similar FEA and analytical software is commonly found in research laboratories, allowing low-cost adoption of this technique. The numerous advantages of the RAFT have been demonstrated. These include: significant reduction in simulation times while accurately including all modes in the response, ability to isolate and attribute contributions to the frequency response of individual modes, ability to attribute coupling to individual piezoelectric components. While this paper was originally inspired by the need to predict spurious modes, other capabilities are now enabled by the RAFT. One such capability is the rapid mode scaling investigations without having to simulate frequency responses. Another would be investigation of nonidealities in the resonator fabrication process.

The technique has been compared to fabricated devices which are one-port, AlN based, and high frequency and

two-port, PZT-on-silicon based as lower frequencies. For the PZT-on-Silicon devices, excellent frequency agreement was seen. For the AlN CLMR resonators, center frequencies were OFF due to the uncertainty in material properties. However, good agreement was demonstrated after scaling the results. The ability to quickly predict resonator coupling as a function of geometric properties was also demonstrated. A key advantage here is ability to predict coupling without simulating a full frequency response, in contrast to other simulation techniques.

Future work will involve including various Q modeling techniques in the RAFT. Accurate quality factor modeling in CMRs is still an area of active research, and therefore experimental Q was used in this paper to validate the RAFT without the extra degree of modeling freedom (i.e., the coupling expression was validated). In addition, adapting the methodology to model other piezoelectric systems (e.g., surface acoustic wave and thin-film bulk acoustic resonators) and other transduction methods (e.g., piezomagnetics and electrostatics) as well is of interest. Thermal loading effects will also be modeled. The methodology used here may also be applied to other resonant systems, such as a piezoelectric gyroscope or a ultrasonic motor.

APPENDIX

The modeling methodology in this section employs comparisons of energy in lumped and distributed systems to arrive at the motional resistance. The derivation is material, mode, and topology agnostic. It is, therefore, a general model, applicable to many systems. A generalized modal force, spring, mass, and capacitor are derived dependent on the strain fields, electric fields, geometric properties, and material properties. The modal (lumped) force is obtained by comparing the strain energy of a spring with an applied force and the strain energy induced by an applied electric field through the piezoelectric material. The modal spring and mass are obtained by comparing the total mechanical energies of each mode of the distributed system with the energy of the simple harmonic oscillator, which is a precept of modal analysis. The charge, and therefore current, on the output electrode is obtained by comparing the energy stored in a lumped capacitor with the energy stored by the induced dielectric displacement in the piezoelectric layer. A transfer function using these elements may be used go from applied voltage to induced strain and finally to output current, or in other words, the motional resistance. Small piezoelectricity is assumed, as discussed in body of this paper.

Modal analysis allows the consideration of one mode independent of all others, and the displacement may be written as a product of the time and spatially dependent components. It may, therefore, be expressed as

$$u = \delta u_n u_t \tag{22}$$

where u_n is the unity normalized mode shape, δ is the zero-frequency displacement amplitude (i.e., maximum displacement) as well as the modal displacement of the lumped

parameter spring, and u_t is the frequency response given by

$$u_{t}(t) = \frac{e^{j\omega t}}{\left[\left(1 - \left(\frac{\omega}{\omega_{n}}\right)^{2}\right) + \frac{\omega}{\omega_{n}Q_{m}}\right]}$$
(23)

where ω is the excitation frequency, ω_n is the natural frequency of the *n*th mode, and Q_m is the mechanical quality factor.

To obtain the modal force, the strain energy created by the applied electric field is compared to the strain energy of a forced spring. This energy may be expressed as

$$PE = \frac{1}{2} \int_{V} T \times S \, dV = \frac{1}{2} k_m \delta^2 \tag{24}$$

where T and S are the 6-D condensed vector representations of stress and strain, respectively, in Voigt's notation, V is the volume of the resonator, and k_m is the modal spring, as obtained by from (11). In this case, the T is the stress caused by the piezoelectric effect, and S is the modal strain. The piezoelectric stress may be obtained from the stress-charge form of the indirect effect piezoelectric constitutive equation

$$T = \mathbf{c}_E \times \mathbf{S} - \mathbf{e}^t \times \mathbf{E}. \tag{25}$$

Here, c_E is the stiffness matrix at constant (zero) electric field, e is the matrix of piezoelectric stress constants, and E is the electric field. Of interest is additional energy introduced into the system from the applied electric field. The stiffness-strain term in (25) account for energy in the system already, and is therefore ignored. Now placing (25) in (24)

$$\frac{1}{2}F_m\delta = \frac{1}{2}k_m\delta^2 = \frac{1}{2}\int_V e^t \times E_{app} \times \delta S_n dV \qquad (26)$$

where F_m is the modal force, k_m is the modal spring, S_n is the strain from the unity normalized mode shape, and E_{app} is the applied electric field. The general modal force may be written

$$F_m = k_m \delta = -\int_{V} e^t \times E_{\rm app} \times S_n dV. \tag{27}$$

The displacement caused by this modal force is then

$$\delta = \frac{F_m}{k_m} = -\frac{\int_V \mathbf{e}^t \times \mathbf{E}_{app} \times \mathbf{S}_n dV}{k_m}.$$
 (28)

For later convenience, (32) may be rewritten with the applied voltage explicitly stated

$$\delta = \frac{F_m}{k_m} = -\frac{\Phi_{\rm in} \int_V e^t \times \nabla \phi_{\rm in} \times S_n dV}{k_m}$$
 (29)

where ϕ_{app} is the magnitude of the applied voltage, and Φ_{in} is the unity normalized electric potential field from the input capacitor, with the ground at 0 potential and the input electrode at a potential of 1.

The real strain may now be expressed as

$$S = \delta S_n u_t = -\frac{\phi_{\text{app}} \int_V \mathbf{e}^t \times \nabla \phi_{\text{in}} \times S_n dV}{k_m} S_n u_t.$$
 (30)

This may be placed in the direct effect equation of the stresscharge form of the piezoelectric constitutive equation

$$\boldsymbol{D} = \boldsymbol{e} \times \boldsymbol{S} + \boldsymbol{\varepsilon}_{S} \times \boldsymbol{E} \tag{31}$$

where D is the induced electric displacement in the piezoelectric layer. The permittivity-electric field term account for electric displacement already present across the output capacitor. The concern is with additional electric displacement generated by the resonator strain, and so the second term is ignored. The energy stored by the direct effect is compared to the energy stored in a "modal" capacitor. The term modal is used here to indicate that the magnitude of the capacitance depends directly on the modal strain. This capacitance, however, is not directly calculated

$$\frac{1}{2} \int_{V} \mathbf{D}_{p} \times \mathbf{E}_{\text{out}} dV = \frac{1}{2} Q_{\text{out}} \Phi_{\text{out}}$$
 (32)

where D_p is the electric displacement from the piezoelectric effect, $E_{\rm out}$ is the electric field resulting on the output electrode, $Q_{\rm out}$ is the charge on the output capacitor, and $\Phi_{\rm out}$ is the magnitude of the voltage across the output port. After writing the electric field once again as the unity normalized potential and voltage magnitude, the charge on the output port may now be written

$$Q_{\text{out}} = \int_{V} \boldsymbol{e} \times \delta \mathbf{S}_{n} \times \nabla \phi_{\text{out}} dV. \tag{33}$$

Now substituting (29) into (33) returns an expression for the charge on the output port dependent upon modal properties, geometry, and material properties only

$$Q_{\text{out}} = \frac{\Phi_{\text{in}} \int_{V} \mathbf{e} \times \mathbf{S}_{n} \times \nabla \phi_{\text{in}} dV \int_{V} \mathbf{e} \times \mathbf{S}_{n} \times \nabla \phi_{\text{out}} dV}{k_{m}}.$$
 (34)

Including (5), taking a time derivative, then absolute value, and setting the frequency to the natural frequency, an expression for the current out of the resonator is obtained

$$I_{\text{out}} = \frac{\Phi_{\text{in}} \omega_n Q_m \left| \int_V \mathbf{e} \times \mathbf{S}_n \times \nabla \phi_{\text{in}} dV \int_V \mathbf{e} \times \mathbf{S}_n \times \nabla \phi_{\text{out}} dV \right|}{k_m}.$$
(35)

Reorganizing to obtain Φ_{in}/I_{out} returns the motional resistance, in agreement with (14)

$$R_{m} = \frac{k_{m}}{Q_{m}\omega_{n} \left| \int_{V} \mathbf{e} \times \mathbf{S}_{n} \times \nabla \phi_{\text{in}} dV \int_{V} \mathbf{e} \times \mathbf{S}_{n} \times \nabla \phi_{\text{out}} dV \right|}.$$
(36)

REFERENCES

- J. M. Puder, J. S. Pulskamp, R. Q. Rudy, R. G. Polcawich, and S. A. Bhave, "Orders of magnitude reduction in acoustic resonator simulation times via the wide-band rapid analytical-FEA technique," in *Proc. IEEE Int. Freq. Control Symp. (IFCS)*, Jul. 2017, pp. 807–810.
- [2] M. Giovannini, S. Yazici, N. K. Kuo, and G. Piazza, "Spurious mode suppression via apodization for 1 GHz AlN contour-mode resonators," in *Proc. IEEE Int. Freq. Control Symp.*, Baltimore, MD, USA, May 2012, pp. 1–5.
- [3] R. H. Olsson, III, K. E. Wojciechowski, and D. W. Branch, "Origins and mitigation of spurious modes in aluminum nitride microresonators," in *Proc. IEEE Int. Ultrason. Symp.*, San Diego, CA, USA, Oct. 2010, pp. 1272–1276.
- [4] D. W. Branch, K. E. Wojciechowski, and R. H. Olsson, III, "Elucidating the origin of spurious modes in aluminum nitride microresonators using a 2-D finite-element model," *IEEE Trans. Ultrason., Ferroelect., Freq. Control*, vol. 61, no. 5, pp. 729–738, May 2014.
- [5] A. Gao and S. Gong, "Harnessing mode conversion for spurious mode suppression in AlN laterally vibrating resonators," *J. Microelectromech. Syst.*, vol. 25, no. 3, pp. 450–458, 2016.

- [6] R. Aigner and L. Elbrecht, "Design and Fabrication of BAW Devices," in RF Bulk Acoustic Wave Filters for Communications, K.-Y. Hashinmoto, Ed. Boston, MA, USA: Artech House, 2009, ch. 4, sec. 1.3, p. 92.
- [7] M. Kamon, "Fast analysis of acoustic resonators for the rapidly growing premium RF filter market," Coventor, Inc., Cary, NC, USA, White Paper, Jun. 2015.
- [8] J. D. Larson, III, R. C. Bradley, S. Wartenberg, and R. C. Ruby, "Modified Butterworth-Van Dyke circuit for FBAR resonators and automated measurement system," in *Proc. IEEE Int. Ultrason. Symp.*, San Juan, PR, USA, vol. 1. Oct. 2000, pp. 863–868.
- [9] J. M. Puder, J. S. Pulskamp, R. Q. Rudy, R. G. Polcawich, and S. A. Bhave, "Fundamental limits of disk flexure resonators," in *Proc. IEEE Int. Freq. Control Symp. (IFCS)*, Jul. 2017, pp. 558–560.
- [10] J. He and Z. Fu, Modal Analysis, 1st ed. Oxford, U.K.: Butterworth, 2001, p. 107.
- [11] J. M. Puder, J. S. Pulskamp, R. Q. Rudy, R. G. Polcawich, and R. G. Polcawich, "A general analytical formulation for the motional parameters of piezoelectric MEMS resonators," *IEEE Trans. Ultrason.*, *Ferroelect., Freq. Control*, vol. 65, no. 3, pp. 476–488, Mar. 2018.
- [12] F. D. Bannon, III, J. R. Clark, and C. T.-C. Nguyen, "High frequency micromechanical filters," *IEEE J. Solid-State Circuits*, vol. 25, no. 4, pp. 512–526, Apr. 2000.
- [13] R. S. A. Wang Bhave and K. Bhattacharjee, "Design and fabrication of S0 Lamb-wave thin-film lithium niobate micromechanical resonators," in *J. Microelectromech. Syst.*, vol. 24, no. 2, pp. 300–308, Apr. 2015.
- [14] G. Piazza, P. J. Stephanou, J. P. Black, R. M. White, and A. P. Pisano, "Single-chip multiple-frequency RF microresonators based on aluminum nitride contour-mode and FBAR technologies," in *Proc. IEEE Ultrason.* Symp., vol. 2. Sep. 2005, pp. 1187–1190.
- [15] R. H. Olsson, III, et al., "Lamb wave micromechanical resonators formed in thin plates of lithium niobate," in Proc. Solid State Sensors, Actuat., Microsyst. Workshop (Hilton Head), Hilton Head Island, South Carolina, 2014, pp. 281–284.
- [16] S. H. Chang, N. N. Rogacheva, and C. C. Chou, "Analysis of methods for determining electromechanical coupling coefficients of piezoelectric elements," *IEEE Trans. Ultrason., Ferroelect., Freq. Control*, vol. 42, no. 4, pp. 630–640, Jul. 1995.
- [17] B. Jaffe, W. R. Cook, and H. Jaffe, "Measurement techniques," in Piezoelectric Ceramics, Marietta, GA, USA: CBLS, ch. 3, sec. 2, p. 31.
- [18] J. S. Pulskamp et al., "Electrode-shaping for the excitation and detection of permitted arbitrary modes in arbitrary geometries in piezoelectric resonators," *IEEE Trans Ultrason.*, Ferroelect., Freq. Control, vol. 59, no. 5, pp. 1043–1060, May 2012.
- [19] J. S. Pulskamp, R. M. Proie, and R. G. Poclawich, "Nano- and microelectromechanical switch dyanmics," *J. Micromech. Microeng.*, vol. 24, no. 1, p. 015011, Dec. 2013.
- [20] H. F. Tiersten, "Expansion in plate eigensolutions," in *Linear Piezo-electric Plate Vibrations*. New York, NY, USA: Plenum, 1969, sec. 3, p. 137.
- [21] E. Elka, D. Elata, and H. Abramovich, "The electromechanical response of multi-layered piezoelectric structures," Technion, Haifa, Israel, Tech. Rep. 478, 2003.
- [22] M. Krommer and H. Irschik, "On the influence of the electric field on free transverse vibrations of smart beams," *Smart. Mater. Struct.*, vol. 8, no. 3, pp. 401–410, 1999.
- [23] J. S. Pulskamp, R. Q. Rudy, S. S. Bedair, J. M. Puder, M. G. Breen, and R. G. Polcawich, "Ferroelectric PZT MEMS HF/VHF resonators/filters," in *Proc. IEEE Int. Freq. Control Symp. (IFCS)*, New Orleans, LA, USA, May 2016, pp. 1–4.
- [24] R. Q. Rudy et al., "Piezoelectric disk flexure resonator with 1 dB loss," in Proc. IEEE Int. Freq. Control Symp. (IFCS), New Orleans, LA, USA, May 2016, pp. 1–4.
- [25] R. G. Polcawich and J. S. Pulskamp, "Additive processes for piezoelectric materials: Piezoelectric MEMS," in *MEMS Materials and Processes Handbook*, R. Ghodssi and P. Lin, Eds. Philadelphia, PA, USA: Springer, 2011, pp. 273–353.
- [26] J. M. Puder, "Modeling of high-electric bias field induced piezoelectric nonlinearity," presented at the Int. Workshop Acoust. Trans. Mater. Devices, Jun. 2016.
- [27] P. Muralt, "AlN thin film processing and basic properties," in *Piezo-electric MEMS Resonators*, H. Bhugra and G. Piazza, Eds. Cham, Switzerland: Springer, 2017, ch. 1, pp. 1–9.
- [28] C. Cassella, "Aluminum nitride cross-sectional lame mode resonators," J. Microelectromech. Syst., vol. 25, no. 2, pp. 275–285, Apr. 2016.

- [29] K. F. Graff, "Wave propagation in rods and plates," in Wave Motion Elastic Solids. New York, NY, USA: Dover, 1975, pp. 440–450.
- [30] C. Cassella, G. Chen, T. Wu, Z. Qian, and M. Rinaldi, "Low impedance arrays of coupled Cross-Sectional Lamé mode resonators with high figure of merit in excess of 100," in *Proc. 19th Int. Conf. Solid-State Sensors, Actuat. Microsyst. (TRANSDUCERS)*, Kaohsiung, Taiwan, Jun. 2017, pp. 1838–1935.
- [31] B. Kim, R. H. Olsson, III, and K. E. Wojciechowski, "AlN microresonator-based filters with multiple bandwidths at low intermediate frequencies," *J. Microelectromech. Syst.*, vol. 22, no. 4, pp. 949–961, Aug. 2013.
- [32] S. Yagnamurthy, I. Chasiotis, J. Lambros, R. G. Polcawich, J. S. Pulskamp, and M. Dubey, "Mechanical and ferroelectric behavior of PZT-based thin films," *J. Microelectromech. Syst.*, vol. 20, no. 6, pp. 1250–1258, Dec. 2011.
- [33] G. Chen, C. Cassella, Z. Qian, G. Hummel, and M. Rinaldi, "Lithographically defined aluminum nitride cross-sectional Lamé mode resonators," J. Micromech. Microeng., vol. 27, no. 3, 2017, Art. no. 034003.
- [34] G. Chen, C. Cassella, T. Wu, and M. Rinaldi, "Single-chip multi-frequency wideband filters based on aluminum nitride Cross-sectional Lamé mode resonators with thick and apodized electrodes," in *Proc. 31st Int. Conf. Micro Electro Mech. Syst. (MEMS)*, Belfast, U.K., Jan. 2018.



Cristian Cassella (S'13–M'15) received the B.S.E. and M.Sc. degrees from the University of Rome Tor Vergata, Rome, Italy, in 2006 and 2009, respectively, and the Ph.D. degree from Carnegie Mellon University, Pittsburgh, PA, USA, in 2015.

In 2011, he joined the University of Pennsylvania, Philadelphia, PA, USA, as a Visiting Scholar. He is currently a Post-Doctoral Researcher with the Electrical and Computer Engineering Department, Northeastern University, Boston, MA, USA. He has authored or co-authored several publications in the

fields of RF MEMS and nonlinear oscillators. His research interests include piezoelectric micro- and nanoelectromechanical systems (M/NEMS) for RF wireless communication systems, the characterization and design of MEM resonators, and design of linear and nonlinear circuits for integrated platforms.

Dr. Cassella received the Best Student Paper Award at the 2013 IEEE International Frequency Control Symposium.



Jonathan M. Puder (S'17–M'17) received the B.S. and M.S. degrees in mechanical engineering from Cornell University, Ithaca, NY, USA, in 2012 and 2016, respectively, where he is currently pursuing the Ph.D. degree in mechanical engineering.

In 2012, he joined with the OxideMEMS Group, Cornell University, as an Undergraduate Research Assistant, where he is currently a Graduate Research Assistant. Since 2014, he has been an ORAU Research Intern with the PiezoMEMS Group, U.S. Army Research Laboratory, Adelphi, MD, USA. His

research interests include piezoelectric MEMS resonance-based devices.



Matteo Rinaldi (S'08–M'10–SM'17) received the Ph.D. degree in electrical and systems engineering from the University of Pennsylvania, Philadelphia, PA, USA, in 2010.

He worked as a Postdoctoral Researcher with the University of Pennsylvania in 2011. In 2012, he joined the Electrical and Computer Engineering Department, Northeastern University, Boston, MA, USA, as an Assistant Professor, where he is currently an Associate Professor with the Electrical and Computer Engineering Department. His

research focuses on understanding and exploiting the fundamental properties of micro/nanomechanical structures and advanced nanomaterials to engineer new classes of micro- and nanoelectromechanical systems (M/NEMS) with unique and enabling features applied to the areas of chemical, physical, and biological sensing and low power reconfigurable radio communication systems. In particular, his group has been actively involved in the experimental research topics and practical applications to ultra-low power MEMS/NEMS sensors (infrared, magnetic, chemical, and biological), plasmonic microand nanoelectromechanical devices, medical microsystems and implantable microdevices for intrabody networks, reconfigurable radio frequency devices and systems, phase change material switches, and 2-D material enabled microand nanomechanical devices. The research in his group is supported by several Federal grants (including DARPA, NSF, and DHS) and the Keck Foundation. He has co-authored over 80 publications in the aforementioned research areas and also holds five patents and more than 10 device patent applications in the field of MEMS/NEMS.

Dr. Rinaldi was a recipient of the IEEE Sensors Council Early Career Award in 2015, the NSF CAREER Award in 2014, and the DARPA Young Faculty Award class of 2012, the Best Student Paper Award at the 2009, 2011, 2015 (with his student), and 2017 (with his student) the IEEE International Frequency Control Symposiums, and the Outstanding Paper Award at the 18th International Conference on Solid-State Sensors, Actuators and Microsystems, Transducers 2015 (with his student).



Jeffrey S. Pulskamp received the B.S. degree in mechanical engineering from the University of Maryland, College Park, MD, USA, in 2000.

He is currently a MEMS Design and Mechanical Engineer with the Micro and Nano Materials and Devices Branch, U.S. Army Research Laboratory, Adelphi, MD, USA. He has authored two book chapters on the design and fabrication of piezoelectric MEMS devices. He holds ten patents related to piezoelectric MEMS devices and has an additional five patents pending. His current research interests

include RF MEMS resonators and switches, electromechanical design and modeling of MEMS, and millimeter-scale robotics.



Ryan Q. Rudy received the B.S.E. and M.S.E. degrees in mechanical engineering from the University of Michigan, Ann Arbor, MI, USA, in 2009 and 2010, respectively, and the Ph.D. degree in mechanical engineering from the University of Maryland, College Park, MD, USA, in 2014, with a focus on miniaturized ultrasonic motors.

He is currently a Mechanical Engineer with the Micro and Nano Materials and Devices Branch, U.S. Army Research Laboratory, Adelphi, MD, USA. His current research interests include piezoelectric

MEMS, specifically piezoelectric electromechanical resonators and filters.



Guofeng Chen (S'16) received the B.E. and M.E. degrees in electrical engineering and automation from the Harbin Institute of Technology, Harbin, China, in 2012 and 2014, respectively. He is currently pursuing the Ph.D. degree in electrical and computer engineering from Northeastern University, Boston, MA, USA.

He has been a Graduate Research Assistant with the Northeastern Sensors and Nano Systems Laboratory, Boston, MA, USA, since 2015. He is currently with the Electrical and Computer Engineering

Department, Northeastern University. His research interests include piezoelectric MEMS resonators, filters, and transformers.



Sunil A. Bhave (S'99–M'05–SM'10) received the B.S. and Ph.D. degrees in electrical engineering and computer science from the University of California at Berkeley, Berkeley, CA, USA, in 1998 and 2004, respectively.

He was with Cornell University, Ithaca, NY, USA, where he was an Associate Professor with the School of Electrical and Computer Engineering for 10 years. In 2015, he joined the Department of Electrical and Computer Engineering, Purdue University, West Lafayette, IN, USA, as an Associate Professor. His

research interests include exploring, understanding, and exploiting interdomain coupling in optomechanical, spin acoustic, and atom-MEMS systems to design inertial sensors, clocks, and field-programmable microwave chipsets.

Dr. Bhave was a recipient of the National Science Foundation Early CAREER Development Award in 2007, the Defense Advanced Research Projects Agency Young Faculty Award in 2008, and the IEEE Ultrasonics Young Investigator Award in 2014. Along with his students, he has been awarded the Roger A. Hakan Best Paper Award at the International Electron Devices Meeting in 2007, and the Student Paper Competition Award at the IEEE International Ultrasonics Symposium in 2009, and the IEEE Photonics Conference in 2012



Ronald G. Polcawich (M'07–SM'16) received the B.S. degree in materials science and engineering from Carnegie Mellon University, Pittsburgh, PA, USA, in 1997, and the M.S. degree in materials and the Ph.D. degree in materials science and engineering from Penn State University, State College, PA, USA, in 1999 and 2007, respectively.

He is currently a Staff Researcher with the Micro and Nano Materials and Devices Branch, U.S. Army Research Laboratory (ARL), Adelphi, MD, USA. He is currently the Team Lead for PiezoMEMS

Technology, ARL, with a focus on developing component technologies to enable cognitive RF communication and radar systems and MEMS inertial and aiding sensors to provide position, navigation, and timing solutions for SWAP-C constrained platforms. He has authored over 70 articles and three book chapters on fabrication and design of piezoelectric MEMS devices using lead zirconate titanate (PZT) thin films. He holds 13 patents and has 10 patent applications pending review. His research activities include materials processing of PZT thin films, MEMS fabrication, RF components, MEMS actuator technologies, millimeter-scale robotics, MEMS inertial sensors, and sensors for aiding inertial systems.

Dr. Polcawich is a member of the IEEE Ferroelectrics Committee and Technical Program Committee IV Applications of Ferroelectrics, served as an Elected Member of the IEEE Ultrasonics, Ferroelectrics, and Frequency Control (UFFC) Administrative Committee for 2014–2016, and has been the Chair of the UFFC Membership Committee since 2016. He was a recipient of the 2012 Presidential Early Career Award for Scientists and Engineers and the 2015 IEEE UFFC Ferroelectrics Young Investigator Award. He is on the Technical Advisory Committee for the PiezoMEMS Workshop, co-organized the 2013 meeting in Washington, DC, USA, and is Co-Organizer for the 2018 meeting in Orlando, FL, USA.